A 2-bit Programmable Metasurface for Dynamic Beam Steering Applications

B. Rezaee Rezvan, M. Yazdi*, S. E. Hosseininejad

Faculty of Electrical and Computer Engineering, Babol Noshirvani University of Technology, Babol, Iran.
behrad7373@nit.ac.ir, yazdi.mohammad@nit.ac.ir, sehosseininejad@nit.ac.ir
*Corresponding author

Received: 2020-10-21
Revised: 2021-01-11
Accepted: 2021-03-14

Abstract
This paper presents a 2-bit programmable digital metasurface for real-time beam steering applications at X-band. Tunability of the metasurface is provided by employing a varactor in the unit cell structure to control each unit cell independently. This ability leads to achieve beam steering capability in both elevation and azimuth directions. The structure is designed so that the biasing circuit has no electrical connection to the MS ground. The equivalent circuit model of the unit cell is also presented to better investigate its physical behaviour. Furthermore, the effects of number of unit cells and states of reflection phase on far-field pattern are investigated. Finally, the numerical results are compared to analytical ones, where a good agreement between them is observed.

Keywords
Programmable metasurface, beam steering, phase profile, varactor.

1. Introduction

Metasurfaces (MSs) are two-dimensional structures consisted of periodic or quasi-periodic elements with subwavelength dimensions called unit cells. They can be used to manipulate electromagnetic (EM) waves with a profound controlling on their behaviour. MS structures have been used in many applications according to their special features. For example, an EM wave absorber was designed for reducing radar cross section in radar application [1] and another MS absorber was implemented in solar cell [2]. A MS was used for linear-to-circular polarization conversion in antenna application [3] and another ultra-wideband polarizer was designed in [4]. A coding MS was designed for reflected beam steering of differently polarized terahertz waves in [5].

These MSs are based on resonant unit cells and therefore have limited operation bandwidth. Thus, the application of these MSs is fixed once they are implemented. Adding tunability to each unit cell provides a reconfigurable MS and expands the abilities and options of MS applications. There are various tuning mechanisms for controlling the EM wave response of the unit cells. For example, graphene and liquid crystal as material tuning, piezoelectric and MEMS switches as geometrical tuning, and Positive–Intrinsic-Negative (PIN) diodes and varactors as circuit tuning approaches. Graphene and liquid crystal change the dielectric coefficient of a unit cell through electrostatic biasing. Graphene is more suitable for applications in terahertz frequencies [6] and liquid crystals can be used at K-band and above. However, liquid crystals have slower response time compared to switches and varactors and are more difficult to implement [7]. The piezoelectric based methods allow limited flexibility proportional to the change in its physical size, which is its drawback [8]. Recently, the MEMS switches arouse attention due to their small size and linearity, but they have relatively slow switching time, compared to the PIN diodes [9]. PIN diodes as switch devices can connect or disconnect conductive elements on the unit cells or between them, thereby two different states of electrical properties of the unit cells can be provided. PIN diodes are conveniently integrated into standard PCB circuits, with fast switching time, high reliability, low cost, and low control voltage switches [10,11]. However, varactors as voltage-controlled capacitances, can prepare more states than PIN diodes due to their continuous tuning capability [12]. Consequently, they are convenient for controlling the resonant frequency of SRRs [13], mushrooms [14] and other types of resonant unit cells. Furthermore, in [14] varactors have been employed to manipulate the phase response of the MS that can be controlled by applying various bias voltages.

The reflection phase of reconfigurable MSs is one of the significant features for applications dealing with reflected EM waves, such as EM wave absorbers [13], reflectarray antennas [14], beam shaping and beam scanning antennas [14-18], lens-based antennas [19], imaging [6], cloaking [20], and holograms [21].

Moreover, simplifying the design procedure and convenient controlling of the unit cells, digital programmable MSs have been presented, which can be controlled by logic devices such as field-programmable gate array (FPGA) in [6,15,17,18,19,21]. Tie J. Cui in 2014 has presented a digital MS with 1-bit controllable unit cells using PIN diodes in [16]. In this paper, a digital

MS with 2-bit controllable unit cell, which is the improved version of 1-bit unit cell proposed in [16], is presented to provide beam steering for both azimuth and elevation angles. In other words, the PIN diode of the unit cell in [16] is replaced by a varactor so that our proposed unit cell is able to cover four states of the reflection phase instead of two states. Furthermore, a new different biasing mechanism is proposed to provide beam steering in both directions. This way, compared to those structures with same application which have more tunable circuit elements in the unit cell, such as [17,18], our structure uses only one tunable circuit element that reduces total costs of metasurface implementation. Furthermore, the unit cell is designed to satisfy local tuning that each unit cell can be tuned independently from adjacent unit cells.

The rest of this paper is structured as follows. The design procedure and the theoretical formulations of beam steering are presented in Section 2. In Section 3, an equivalent circuit model of the proposed MS and an analytical approach for analyzing the MS response are provided. Moreover, a discussion about parameters that affect the beam steering properties, and the simulation results compared to analytical ones for the evaluation are presented. In the last part of this section, the performance results of the proposed MS are compared using full wave and analytical simulations. Finally, the paper is concluded in section 4.

2. Theory and Design

To illustrate the design approach of MS with 2-bit controllable unit cells for beam steering applications, the theory formulation of the MS performance is desired. In Section 2.1, the formulations describing relation between the desired direction and the phase profile of MS**,** are developed. Next in Section 2.2 the design process of the MS is comprehensively described. Then, the proposed unit cell structure which provides four different states of the reflection phase is presented in Section 2.3.

2.1. Generalized Reflection Law Formulation

In beam steering applications, the direction of the reflected beam can be controlled by a variation in the phase profile of the reflective surface, as schematically depicted in Fig. 1. The formulation of the beam steering will be derived based on the generalized reflection law [24].

Considering the phase profile of the MS, the relation between incident $\vec{\boldsymbol{k}}_{\boldsymbol{i}}$ and reflected $\vec{\boldsymbol{k}}_{\boldsymbol{r}}$ wave vectors can be obtained as:

$$\vec{\boldsymbol{k}}_{\boldsymbol{i}} - \vec{\boldsymbol{k}}_{\boldsymbol{r}} = \nabla \boldsymbol{\Phi}(x,y) \quad (1)$$

where, $\boldsymbol{\Phi}(x,y)$ is the phase profile of the reflective surface in the *x*-*y* plane and ∇ indicates gradient operator. The reflected wave vector $\vec{\boldsymbol{k}}_{\boldsymbol{r}}$, according to the coordinate system shown in Fig. 1, can be written as:

$$k_{rx} = k_r \sin\theta_r \cos\varphi_r \quad (2)$$

$$k_{ry} = k_r \sin\theta_r \sin\varphi_r \quad (3)$$

$$k_{rz} = k_r \cos\theta_r \quad (4)$$

The same formulation can also be applied to the incident wave. Eq. (1) can be separated into x and y components using (2-4) as:

$$k_r \sin\theta_r \cos\varphi_r - k_i \sin\theta_i \cos\varphi_i = \frac{d\boldsymbol{\Phi}(x,y)}{dx} \quad (5)$$

$$k_r \sin\theta_r \sin\varphi_r - k_i \sin\theta_i \sin\varphi_i = \frac{d\boldsymbol{\Phi}(x,y)}{dy} \quad (6)$$

Considering normal incident wave ($\theta_i = \varphi_i = 0$) on the MS in free space ($k_i = k_r = 2\pi/\lambda_0$), and by solving (5,6), the elevation angle θ_r and azimuth angle φ_r of the reflected beam are obtained as:

$$\theta = sin^{-1}\left(\frac{\lambda_0\sqrt{(d\boldsymbol{\Phi}/dx)^2 + (d\boldsymbol{\Phi}/dy)^2}}{2\pi}\right) \quad (7)$$

$$\varphi = tan^{-1}\left(\frac{d\boldsymbol{\Phi}/dy}{d\boldsymbol{\Phi}/dx}\right) \quad (8)$$

which relates the phase profile of the MS to the direction of the reflected wave.

2.2. Design Flow

The design process of MS for beam steering application can be described based on (7,8). Calculation of the phase profile $\boldsymbol{\Phi}(x,y)$ is needed to achieve the desired elevation and azimuth angles of the reflected wave. The phase profile is actually a discretised function, because each unit cell has a uniform phase shifting value over its dimension (p). To apply this condition, we consider $\Delta\boldsymbol{\Phi}$, Δx and Δy instead of $d\boldsymbol{\Phi}$, dx and dy in (5,6). Thus, the distance between unit cells with different states, Δx and Δy, can be obtained using (5,6) as:

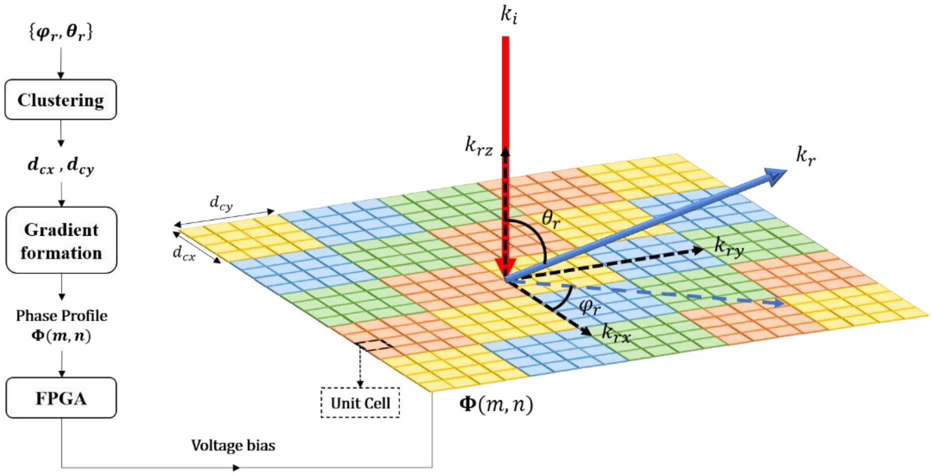

Fig. 1. Design flow of the proposed 2-bit programmable MS: In clustering step, the discretised cluster sizes d_{cx}, d_{cy} are obtained using the desired direction of reflected beam. In gradient formation step, the phase profile of the MS is calculated, then using FPGA the biasing voltage of each cluster is applied

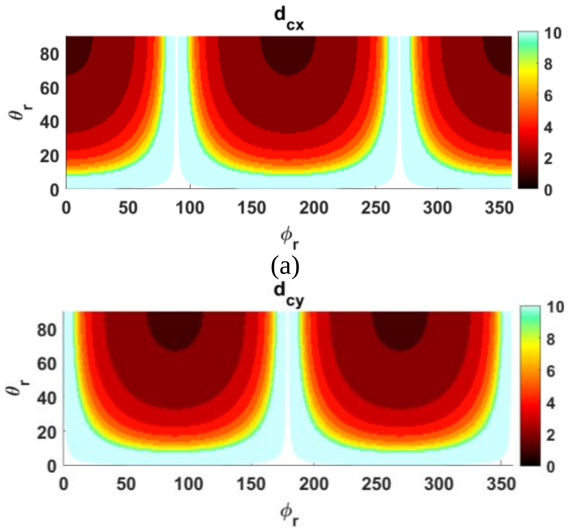

Fig. 2. Absolute values of (a) d_{cx} and (b) d_{cy}, as functions of desired direction of the reflected beam.

$$\Delta x = \frac{\lambda_0 \Delta\Phi}{2\pi \sin\theta_r \cos\varphi_r} \tag{9}$$

$$\Delta y = \frac{\lambda_0 \Delta\Phi}{2\pi \sin\theta_r \sin\varphi_r} \tag{10}$$

Applying a value for the number of bits (n), the phase difference required in each unit cell would be: $\Delta\Phi = 2\pi/2^n$. Substituting $\Delta\Phi$ in (9,10), the cluster sizes of c_x and c_y that are number of a collection of adjacent unit cells with same state, can be obtained as:

$$c_x = \lambda_0/(2^n \sin\theta_r \cos\varphi_r) \tag{11}$$

$$c_y = \lambda_0/(2^n \sin\theta_r \sin\varphi_r) \tag{12}$$

Since the unit cells have fixed dimensions, the discretised cluster size or the required number of unit cells in a single cluster is easily calculated as:

$$d_{cx} = \left\lfloor \frac{c_x}{p} \right\rceil \quad , \quad d_{cy} = \left\lfloor \frac{c_y}{p} \right\rceil \tag{13}$$

where ⌊ ⌉ is the rounding operation. Considering $\Delta x = mp$ ($m = 1, 2, \ldots, M$) and $\Delta y = np$ ($n = 1, 2, \ldots, N$), where M and N are respectively the total number of unit cells in the x and y directions. The phase profile $\boldsymbol{\Phi}(m,n)$ can then be expressed as:

$$\boldsymbol{\Phi}(m,n) = \frac{2\pi}{2^n} \times \left[\left(\left\lfloor \frac{m}{d_{cx}} \right\rceil + \left\lfloor \frac{n}{d_{cy}} \right\rceil\right) \%2^n\right] \tag{14}$$

where % is the modulo operation.

The full design process of a 2-bit digital MS is summarized in Fig. 1. In the clustering step the desired direction of the reflected beam $\{\varphi_r, \theta_r\}$ is applied to (11,12) and then the discretised cluster size $\{d_{cx}, d_{cy}\}$ can be obtained using (13). The gradient formation of the phase profile on MS, $\boldsymbol{\Phi}(m,n)$ can be achieved using (14). Finally, the bias voltage of each unit cell, according to the phase profile, is applied using a logic device such as FPGA to the biasing circuit that is implemented on the back plane of the MS.

Figure 2 shows absolute values of d_{cx} and d_{cy} as functions of the desired direction of the reflected beam for a normally incident plane wave. As it can be seen, for some cases of θ_r and φ_r, the number of unit cells in a single cluster goes to infinity which means that the phase profile has no variations in the particular axis. However, in some directions where c_x or c_y are smaller than p, the distance parameters of d_{cx} or d_{cy} would be zero, which are not feasible and also limits the upper range of states.

2.3. The Proposed Unit Cell Design

The proposed tunable unit cell structure is inspired from [16]. As shown in Fig. 3, this structure is composed of two patches etched on a substrate with ε_r=2.2 and 2 mm thickness (rogers RT5880) on a ground plane. Patches and ground are made up of copper with 0.017 mm thickness. A MAVR-011020-1141 varactor is deployed between two patches. The varactor has constant gamma (γ) factor in the range of the biasing voltage which provides linear tuning capability [12].

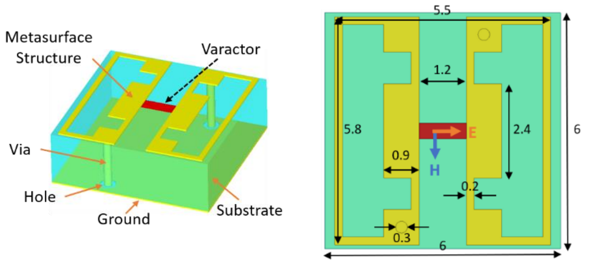

(a) (b)

Fig. 3. Unit cell structure (a) perspective view, (b) top view and dimensions

Compared to [16], a different biasing mechanism is used here. Biasing mechanism in [16] is provided through vias by a DC voltage connected to the ground plane and two leads of PIN diode separated by a gap in the ground plane. The shape of the ground in [16], indicates that all unit cells in a same column are biased simultaneously but independently in rows. Therefore, regardless of limitation of number of states that limits the application, in beam steering application using such biasing mechanism, this design can only change the direction of reflected beam only in elevation or azimuth angle but not both.

Here, in the proposed structure, an entire metallic sheet with two holes is used as ground of the unit cell. These holes are adjusted for biasing the varactor through the vias separately and without electrical connection to the ground, to have beam steering in both directions. The radius of these holes is chosen twice bigger than radius of vias. One important point about the proposed unit cell is that it is uses only one tunable circuit element that reduces costs of MS implementation compared to those structures with same application which have more tunable circuit elements in the unit cell [17,18].

The selected varactor can provide a variable capacitance with range of 0.025 pF to 0.19 pF corresponded to 15 V and 0 V bias voltages respectively, with parasitic impedances. Thus, to find different states of the unit cell for beam steering application, four different cases corresponded to four different bias voltages of the varactor have been simulated. The full-wave simulation results are obtained using the commercial software CST Microwave Studio 2019.
The reflected amplitudes and phases of the structure in four cases are depicted in Fig. 5. The polarization of incident and reflected wave is according to Fig. 3(b). As can be seen, at 9 GHz centre frequency, this unit cell covers four states of the reflected phase (“00”, ”01”, ”10” and “11” states) which are approximately 0, 90, 180 and 270 degrees, by applying different bias voltages. Values of bias voltages and total capacitances related to different states are mentioned in Table I.

Table I. States and characteristics of the unit cell

	State 00	State 01	State 10	State 11
Phase (°)	0	90	180	270
C_t (pF)	0.058	0.025	0.11	0.072
V_b (V)	6	15	2	4

3. Results and Discussion

This section is devoted to the analyzing and modelling of the proposed structure. In section 3.1, an equivalent circuit model of the unit cell is provided to describe the physical structure using circuitry elements. In section 3.2, the analytical approach for analyzing the response of the MS with a comprehensive discussion about the effects of number of unit cells and states, on the far-filed pattern is provided. Finally, to evaluate the design process introduced in section 2.2, a comparison between numerical and analytical simulation results of beam steering is presented in section 3.3.

3.1. Equivalent circuit model

Here, an equivalent circuit model of the unit cell is provided to describe the physical behavior of the structure using circuit components, as depicted in Fig. 4. In this model, the media of propagation of the incident plane waves is modelled by a transmission line with characteristic impedance of $Z_0 = \eta_0 = 377$ ohms. The patch structure of the unit cell behaves as RLC circuit and the implemented varactor is placed parallel to the capacitance.

According to [13], the substrate is modelled as an inductor L_d and the end of the circuit is loaded by a short circuit because of the presence of the ground plane. Therefore, the impedance $Z(\omega)$ represents the surface impedance of the unit cell. The parasitic impedances of the varactor are considered in series resistance and inductance (R and L). Values of each parameter of circuit model for different states are mentioned in Table II. It should be noted that although there are approximate formulas for calculating the values of the model, but exact values are extracted using the optimization and tuning by a circuit simulator (Advanced Design System (ADS)).

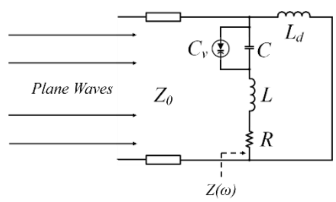

Fig. 4. The proposed circuit model of the unit cell

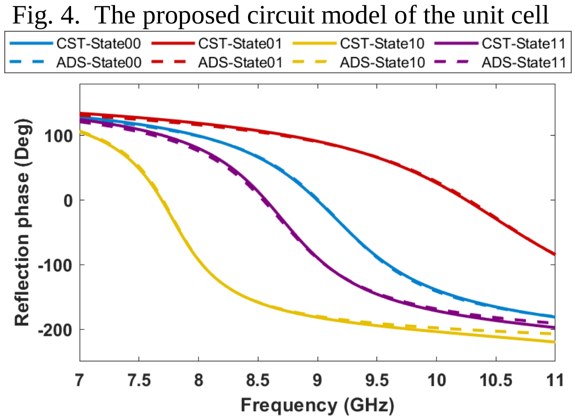

(a)

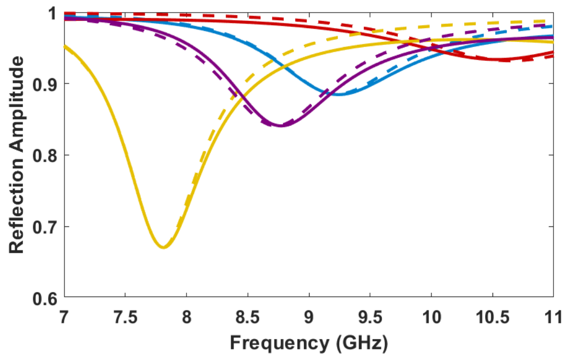

(b)

Fig. 5. Comparison of (a) reflection phase and (b) reflection amplitude, of full wave simulation results (using CST) and equivalent circuit model (using ADS) of the proposed unit cell in different states.

Table II. Parameter values of circuit model

	State 00	State 01	State 10	State 11
R (Ohm)	3.825	2.8	8.742	4.95
C (pF)	0.001	0.001	0.001	0.001
C_v (pF)	0.034	0.0314	0.04	0.038
L (nH)	6	4.5	7.6	6
L_d (nH)	2.9	2.9	2.9	2.8

The reflected amplitude and phase of the equivalent circuit model compared to full wave simulation results obtained by CST are depicted in Fig. 5. As can be observed, the introduced circuit effectively models the behaviour of the proposed unit cell in the entire band and therefore can be used to predict and analyze the behaviour of the proposed unit cell.

3.2. Analytical Approach

This subsection is aimed to present the analytical formulation of far-field scattering pattern of the MS, $\boldsymbol{F}(\varphi,\theta)$. From antenna array theory [15] on can write:

$$\boldsymbol{F}(\varphi,\theta) = \boldsymbol{f_E}(\varphi,\theta) \times \boldsymbol{f_A}(\varphi,\theta) \tag{15}$$

where $\boldsymbol{f_E}(\varphi,\theta)$ and $\boldsymbol{f_A}(\varphi,\theta)$ are element factor (pattern function of single unit cell) and array factor (pattern function of unit cell arrangement), respectively. By assuming an $M\times N$ MS with element factor as dipolar scatterer, i.e. $\boldsymbol{f_E}(\varphi,\theta) = \cos\theta$ [19], and the phase profile $\boldsymbol{\Phi}(m,n)$ to be exactly either 0, 90, 180, or 270 degrees, $\boldsymbol{F}(\varphi,\theta)$ can be obtained as:

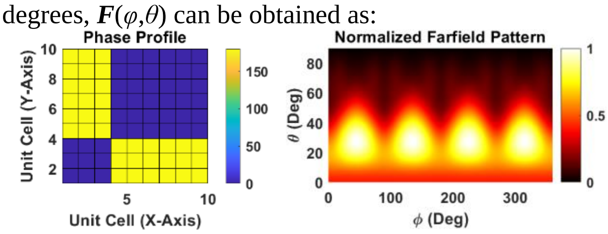

(a)

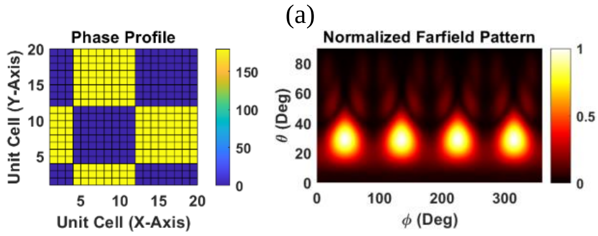

(b)

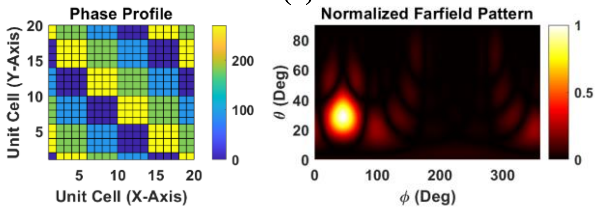

(c)

Fig. 6. The phase profile and the normalized far-field scattering pattern of MS with: (a) M = N = 10, n = 1, (b) M = N = 20, n = 1, (c) M = N = 20, n = 2.

$$\begin{aligned}\boldsymbol{F}(\varphi,\theta) = \cos\theta \sum_{m=1}^{M}\sum_{n=1}^{N} & \exp(-j[\boldsymbol{\Phi}(m,n) \\ & + kp(m-0.5)\sin\theta\cos\varphi \\ & + kp(n-0.5)\sin\theta\sin\varphi]) \end{aligned} \tag{16}$$

To investigate effects of number of unit cells (M and N) and number of states (n) on the far-field scattering pattern, the $\boldsymbol{F}(\varphi,\theta)$ function calculated for different values of these parameters using (16).

Figure 6 shows different phase profile and normalized far-field patterns which in all cases the normally incident plane wave and $\theta_r = 30°$, $\varphi_r = 45°$ have been considered. It can be understood from Fig. 6 that the beamwidth decreases by increasing number of unit cells (M and N). It also can be seen that the level of grating lobes decreases by increasing the number of states. Another important point from Fig. 6 is that for beam steering capability, the number of states must be selected more than two ($n > 1$).

3.3. Numerical Results

In the previous subsection, the unit cells are assumed to have fixed reflection phases and unit reflection amplitudes and then, the far-field pattern calculated analytically. To evaluate the beam steering applicability of the MS in the real world, i.e., with distributed reflection phase and amplitudes of unit cells and also assuming interference between them, the full wave simulation for a MS with 20×20 unit cells which introduced in section 2.3, is presented. There are two cases to evaluate this design: Case 1: beam steering in θ direction. Case 2: beam steering in φ direction.

Therefore, four different θ_r values for case 1 and four different φ_r values for case 2 are considered as the desired directions of the reflected beam. The analytical and numerical (full wave simulation) results of normalized far-field patterns are depicted in Fig. 7 and Fig. 8, respectively. In all cases normally incident plane wave is considered. It can be seen from Fig. 7(a-d) and Fig. 8(a-d) for case 1 that the θ_r of the main beam steered approximately from 0° to 60° by 20° steps. Also, Fig. 7(e-h) and Fig. 8(e-h) shows that φ_r steered almost from 40° to 310° by 90° steps for case 2.

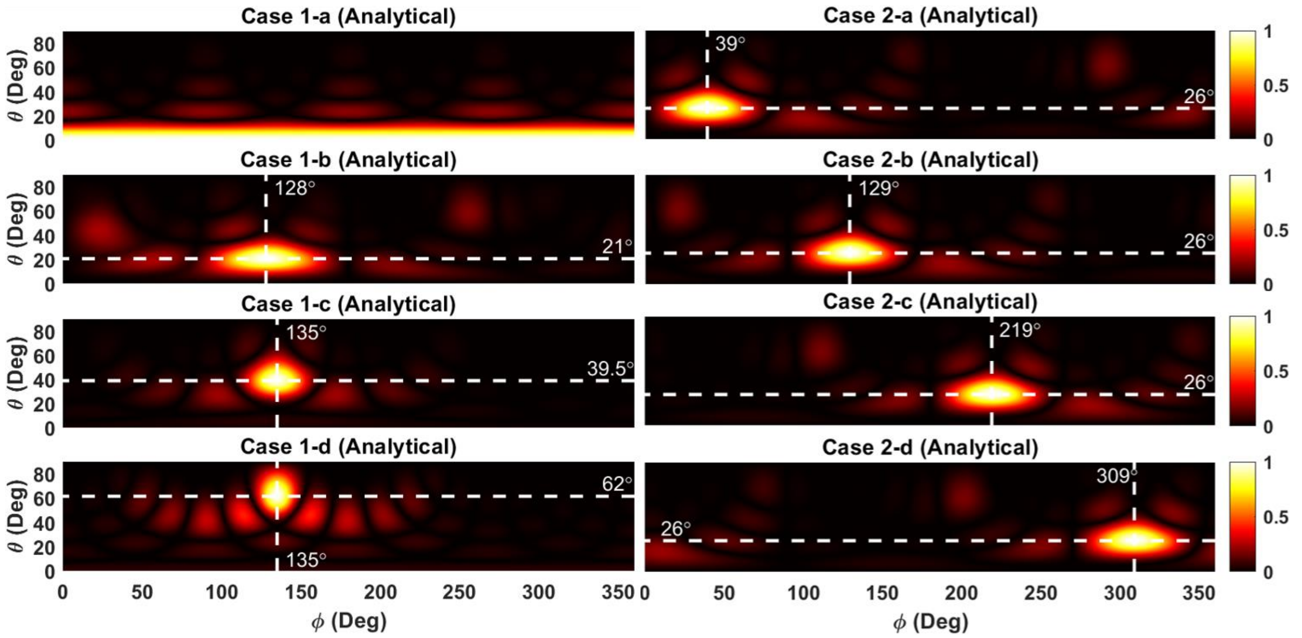

Fig. 7. The normalized far-filed scattering pattern of analytical results of (left column) case 1 with (first row) $\theta_r = 0°$, (second row) $\theta_r = 20°$, (third row) $\theta_r = 40°$, (fourth row) $\theta_r = 60°$ and consant $\varphi_r = 135°$ as desired directions, and (right column) case 2 with (first row) $\varphi_r = 40°$, (second row) $\varphi_r = 130°$, (third row) $\varphi_r = 220°$, (forth row) $\varphi_r = 310°$ and consant $\theta_r = 30°$ as desired directions.

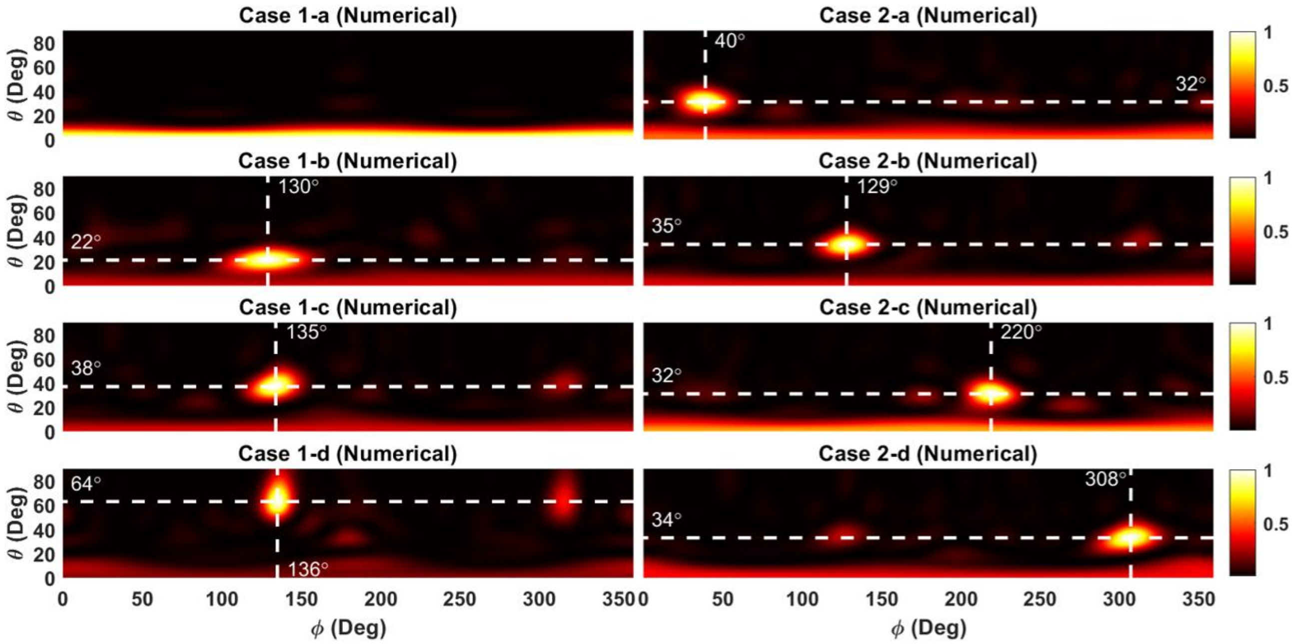

Fig. 8. The normalized far-filed scattering pattern of numerical simulation results of (left column) case 1 with (first row) $\theta_r = 0°$, (second row) $\theta_r = 20°$, (third row) $\theta_r = 40°$, (forth row) $\theta_r = 60°$ and consant $\varphi_r = 135°$ as desired directions, and (right column) case 2 with (first row) $\varphi_r = 40°$, (second row) $\varphi_r = 130°$, (third row) $\varphi_r = 220°$, (forth row) $\varphi_r = 310°$ and consant $\theta_r = 30°$ as desired directions.

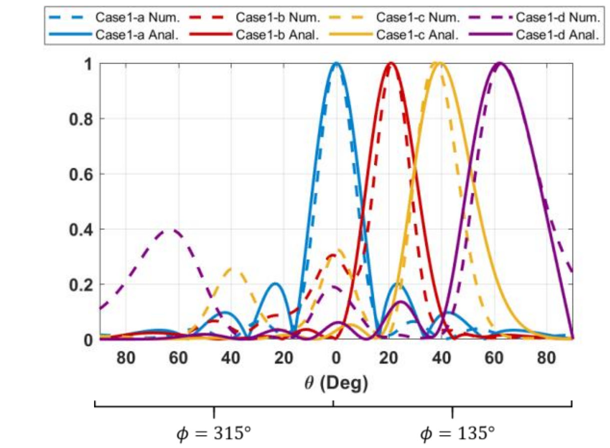

(a)

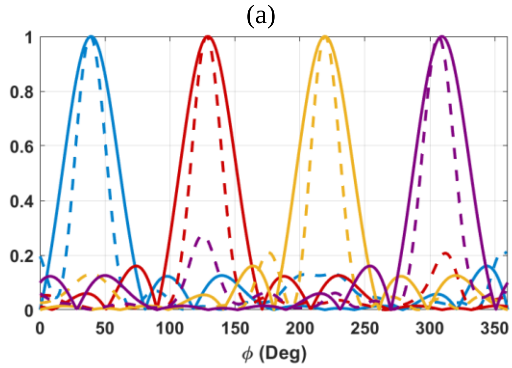

(b)

Fig. 9. The normalized far-field scattering patterns of numerical and analytical simulations of (a) case 1 with θ_r = 0°, 20°, 40°, 60° and consant φ_r = 135° and (b) case 2 with φ_r = 40°, 130°, 220°, 310° and consant θ_r = 30° desired directions.

Figure 9 (a) and (b) respectively illustrate normalized far-field scattering patterns corresponding to constant φ values for case 1 and constant θ values for case 2. As can be seen, there is fair agreement between analytical and numerical results. However, in the numerical results, more side lobes along with main lobe have been appeared as a consequence of the interference between unit cells. Also, main beam directions in these results have been slightly deviated from the desired directions which occur at a result of discretization of the phase profile. The desired and simulated main beam directions with the steering error evaluated as the difference between desired and achieved main beam direction for each case are given in Table III. As can be observed in this table, the steering error is not exceeded from 5° in the worst case.

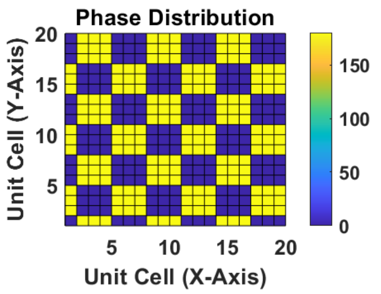

(a)

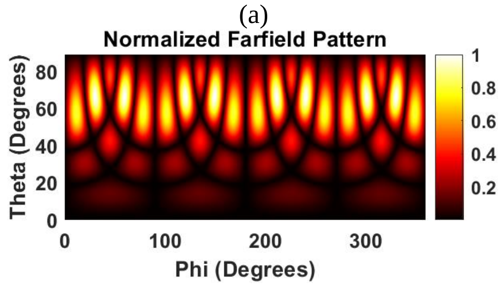

(b)

Fig. 10. The MS designed for RCS reduction: (a) the phase distribution and (b) normalized farfield pattern

The proposed unit cell in this paper can be also applied for the application of radar cross section (RCS) reduction. So, here we present the results of this feature.

Table III. Performance Results

		Beam Steering in θ				Beam Steering in φ			
		Case 1-a	Case 1-b	Case 1-c	Case 1-d	Case 2-a	Case 2-b	Case 2-c	Case 2-d
Desired Direction $\{\varphi_r(°), \theta_r(°)\}$		{- , 0}	{130,20}	{130,40}	{130,60}	{40,30}	{130,30}	{220,30}	{310,30}
Achieved main beam $\{\varphi_{ra}(°), \theta_{ra}(°)\}$	Anal.	{- , 0}	{128,21}	{135,39.5}	{135,62}	{39,26}	{129,26}	{219,26}	{309,26}
	Num.	{- , 0}	{130,22}	{135,38}	{136,64}	{40,32}	{129,35}	{220,32}	{308,34}
Error of direction $\{Err_\varphi(°), Err_\theta(°)\}$	Anal.	{- , 0}	{2,1}	{5,0.5}	{5,2}	{1,4}	{1,4}	{1,4}	{1,4}
	Num.	{- , 0}	{0,2}	{5,2}	{6,4}	{0,2}	{1,5}	{0,2}	{2,4}

The RCS is defined as the ratio of the backscattered wave to the incident wave. One RCS reduction technique is to guide the reflected wave to other directions that do not point to the receivers. The RCS reduction in [16] is based on this technique and it is obtained using the chessboard pattern of the phase profile of MS. Therefore, we present the results of RCS reduction of our proposed MS by this approach. The phase profile is chosen to be chessboard pattern as depicted in Fig. 10(a) and the normalized farfield pattern of the MS according to normal incident is shown in Fig. 10(b). As it can be seen the power of reflection wave is splitted and scattered from the broadside angle into other angles.

4. Conclusion

This paper proposes a 2-bit programmable MS structure by means of varactors for 2D beam steering application at 9 GHz frequency. Beam steering is achieved in both elevation and azimuth directions by independently controlling the unit cells in a digital manner. The unit cell structure presented in this paper can be tuned locally and independent from adjacent unit cells. It is shown that for beam steering, unit cells must provide more than two phase states and the beam width can be reduced by using more unit cells (bigger MS size). An equivalent circuit model of the unit cell is provided. The numerical and analytical simulation results are presented to evaluate the design process and a good agreement between them is achieved.

5. Acknowledgement

The authors acknowledge the funding support of Babol Noshirvani University of Technology through Grant program No. BNUT/391025/99.

6. References

[1] R. Sekar, S.R. Inabathini, “An ultra-thin compact wideband metamaterial absorber”, *Radioengineering*, vol. 27, no. 2, p. 365, 2018.

[2] P. Rufangura, C. Sabah, “Wide-band polarization independent perfect metamaterial absorber based on concentric rings topology for solar cells application”, *Journal of Alloys and Compounds*, vol. 680 pp. 473-479, 2016.

[3] H. L. Zhu, S.W. Cheung, K.L. Chung, T.I. Yuk, “Linear-to-circular polarization conversion using metasurface”, *IEEE Transactions on Antennas and Propagation*, vol. 61, no. 9 pp. 4615-4623, 2013.

[4] J. Y. Yin, X. Wan, Q. Zhang, and T. J. Cui, “Ultra Wideband polarization-selective conversions of electromagnetic waves by metasurface under large-range incident angles”, *Scientific reports*, vol. 5, p. 12476, 2015.

[5] S. Liu, T.J. Cui, Q. Xu, D. Bao, L. Du, X. Wan, W.X. Tang, C. Ouyang, X.Y. Zhou, H. Yuan, H.F. Ma, “Anisotropic coding metamaterials and their powerful manipulation of differently polarized terahertz waves”, *Light: Science & Applications*, vol. 5, no. 5, pp. e16076-e16076, 2016.

[6] S.E. Hosseininejad, K. Rouhi, M. Neshat, R. Faraji-Dana, A. Cabellos-Aparicio, S. Abadal, E. Alarcón, “Reprogrammable graphene-based metasurface mirror with adaptive focal point for THz imaging”, *Scientific reports*, vol. 9, no. 1, pp. 1-9, 2019.

[7] P. Yaghmaee, O. H. Karabey, B. Bates, C. Fumeaux, and R. Jakoby, “Electrically tuned microwave devices using liquid crystal technology”, *International Journal of Antennas and Propagation*, 2013.

[8] M. Mavridou, A.P. Feresidis, “Dynamically reconfigurable high impedance and frequency selective metasurfaces using piezoelectric actuators”, *IEEE Transactions on Antennas and Propagation*, vol. 64, no. 12, pp. 5190-5197, 2016.

[9] Tian, Wenchao, Ping Li, and LinXiao Yuan, “Research and analysis of MEMS switches in different frequency bands”, *Micromachines*, vol. 9, no. 4, pp. 185, 2018.

[10] S.V. Hum, J. Perruisseau-Carrier, “Reconfigurable reflectarrays and array lenses for dynamic antenna beam control: A review”, *IEEE Transactions on Antennas and Propagation*, vol. 62, no. 1, pp. 183-198, 2013.

[11] Solderable AlGaAs Flip Chip PIN. Available online: https://cdn.macom.com/datasheets/MADP-000907-14020x.pdf (accessed on 11 June 2020).

[12] MACOM. MAVR-011020-1411, Solderable GaAs Constant Gamma Flip-Chip Varactor Diode. Available online: https://cdn.macom.com/datasheets/MAVR-011020-1141.pdf (accessed on 11 June 2020).

[13] J. Zhu, D. Li, S. Yan, Y. Cai, Q.H. Liu, T. Lin, “Tunable microwave metamaterial absorbers using varactor-loaded split loops”, *EPL Europhysics Letters*, vol. 112, no. 5, pp. 54002, 2015.

[14] D.F. Sievenpiper, J.H. Schaffner, H.J. Song, R.Y. Loo, G. Tangonan, “Two-dimensional beam steering using an electrically tunable impedance surface”, *IEEE Transactions on Antennas and Propagation*, vol. 51, no. 10, pp. 2713-2722, 2003.

[15] S.E. Hosseininejad, K. Rouhi, M. Neshat, A. Cabellos-Aparicio, S. Abadal, E. Alarcón, “Digital metasurface based on graphene: an application to beam steering in terahertz plasmonic antennas”, *IEEE Transactions on Nanotechnology*, vol. 18, pp. 734-746, 2019.

[16] T.J. Cui, M.Q. Qi, X. Wan, J. Zhao, Q. Cheng, "Coding metamaterials, digital metamaterials and programmable metamaterials." *Light: Science & Applications*, vol. 3, no. 10, pp. e218-e218, 2014.

[17] C. Huang, B. Sun, W. Pan, J. Cui, X. Wu, X. Luo, “Dynamical beam manipulation based on 2-bit digitally-controlled coding metasurface”, *Scientific reports*, vol. 7, no. 1, pp. 1-8, 2017.

[18] Q. Ma, G.D. Bai, H.B. Jing, C. Yang, L. Li, T.J. Cui, “Smart metasurface with self-adaptively reprogrammable functions”, *Light: Science & Applications*, vol. 8, no. 1, pp. 1-12, 2019.

[19] H. Yang, X. Cao, F. Yang, J. Gao, S. Xu, M. Li, X. Chen, Y. Zhao, Y. Zheng, S. Li, “A programmable metasurface with dynamic polarization, scattering and focusing control”, *Scientific reports*, vol. 6, n. 35692, 2016.

[20] S. Liu, H.X. Xu, H.C. Zhang, T.J. Cui, “Tunable ultrathin mantle cloak via varactor-diode-loaded metasurface”, *Optics express*, vol. 22, no. 11, pp. 13403-13417, 2014.

[21] L. Li, T.J. Cui, W. Ji, S. Liu, J. Ding, X. Wan, Y.B. Li, M. Jiang, C.W. Qiu, S. Zhang, “Electromagnetic reprogrammable coding-metasurface holograms”, *Nature communications*, vol. 8, no. 1, pp. 1-7, 2017.

[22] N. Yu, P. Genevet, M.A. Kats, F. Aieta, J.P. Tetienne, F. Capasso, Z. Gaburro, “Light propagation with phase discontinuities: generalized laws of reflection and refraction”, *Science*, vol. 334, no. 6054, pp. 333-337, 2011.

[23] رضا اصغریان، بیژن ذاکری، محمد یزدی، ستار صمدی، «طراحی آنتن آرایه انعکاسی هدایت‌گر پرتو غیرفعال با استفاده از عناصر غیریکنواخت به‌منظور بهبود پهنای پرتو اصلی و سطح گلبرگ جانبی»، *مجله مهندسی برق دانشگاه تبریز*، دوره ۴۹، شماره ۳، صفحه ۹۹۳-۹۸۵، ۱۳۹۸

[24] زهرا حبیبی، مرتضی کازرونی، سید حسین محسنی ارمکی، عماد حمیدی، «ارائه یک روش کاربردی جهت کالیبراسیون آنتن‌های آرایه فازی»، *مجله مهندسی برق دانشگاه تبریز*، دوره ۴۵، شماره ۴، صفحه ۸۴-۷۹، ۱۳۹۴